Hot corrosion of modified Ti₃Al-based alloy coated with thin Na₂SO₄ film at 910 and 950 °C in air

Yu-hai QIAN[1], Xi-chao LI[1,2], Mei-shuan LI[1], Jing-jun XU[1], Bin LU[1]

1. Shenyang National Laboratory for Materials Science, Institute of Metal Research,
Chinese Academy of Sciences, Shenyang 110016, China;
2. University of Chinese Academy of Sciences, Beijing 100039, China

Abstract: The hot corrosion behaviour of a modified Ti₃Al-based alloy under thin Na₂SO₄ deposit film was investigated at 910 and 950 °C in air. The corrosion product was identified by XRD and its morphologies on the surface and cross-section were observed by SEM. The alloy suffered from considerable hot corrosion attack. The mass gain versus time curves obtained by TGA exhibited two regions of different kinetics. The whole corroded layer consisted of loose and porous mixture oxides of TiO₂, Nb₂O₅ and Al₂O₃. Numerous small nodules of corrosion product were observed. An illustrative schematic was established to describe the formation process of such nodules. It seemed that the refractory oxides played a significantly important role in determining the development of hot corrosion attack.

Key words: modified Ti₃Al-based intermetallics; hot corrosion; corrosion product nodule; Na₂SO₄ melt

1 Introduction

With considerably attractive combination of both excellent physical properties and mechanical properties, such as relatively low density, high specific strength and high elastic modulus at elevated temperatures, intermetallics such as Ti₃Al and TiAl are concerned extensively [1−3]. They might act as potential high temperature structural materials for aeroengine and automobile parts [4−9]. However, the poor oxidation resistance at high temperatures strongly limits their practical application. For example, creep resistance of Ti₃Al is maintained up to 815 °C, but its oxidation resistance is poor at and above 650 °C [10]. Theoretical analysis [11,12] and experimental studies [13,14] revealed that non-protective oxide scales are produced when aluminum content is lower than 50% (mole fraction) for Ti−Al intermetallic compounds.

Considering the practical service environment at high temperatures, more attention has been paid to the high-temperature oxidation resistance of aluminide intermetallics [15,16]. It is revealed that the oxidation resistance of Ti₃Al intermetallic compounds is significantly poor at higher temperatures [17,18], because a mixture of oxides consisting of TiO₂ and Al₂O₃ rather than a single protective Al₂O₃ layer was produced on Ti₃Al-based alloys due to relatively low Al content [19]. Meanwhile, their oxidation kinetics was drastically complicated due to both the rapid diffusivity and high dissolution ability of oxygen both in the oxide layer and the substrate [12,13,20−26].

Addition of alloying elements (such as Nb, Mo and V) is an essential way to improve oxidation resistance of titanium−aluminide intermetallics [6,22,27,28]. However, their application at high temperatures is commonly exposed to environments containing molten salts, e.g., sodium sulphate (Na₂SO₄), especially under the combustion environments [29]. It is suggested that components of titanium alloys experience severe hot corrosion attack when the aircraft flies at low altitudes across the sea [30]. But investigations on hot corrosion resistance of Ti₃Al intermetallics still keep scarce up to now. A better understanding of hot corrosion behaviour is very vital to their viable application. As an intermetallic compound modified with β-stabilizing alloying elements, Ti−24Al−14Nb−3V−0.5Mo−0.3Si (mole fraction, %) is of great interest for its application in industrial and

aero-gas turbine engines at high temperatures. But its hot corrosion resistance is still not understood.

In the present study, the hot corrosion behaviour of the Ti−24Al−14Nb−3V−0.5Mo−0.3Si (mole fraction, %) alloy coated with a load of about 3 mg/cm^2 Na$_2$SO$_4$ on its surfaces at 910 and 950 °C in air was investigated. The hot corrosion kinetics, phase composition, microstructure and morphology of corrosion product were characterized. And a possible mechanism of hot corrosion was proposed as well.

2 Experimental

The Ti$_3$Al-based alloy ingot with nominal composition of Ti−24Al−14Nb−3V−0.5Mo−0.3Si (mole fraction, %) was prepared by melting twice in a consumable-electrode arc furnace under vacuum. Billets were obtained from the ingots. After hot press forging first in the β-phase region at 1200 °C, they were intermediately annealed in the $(\alpha_2+\beta_2)$ two-phase region at 1050 °C. The heat treatment schedule of the alloy after forging was (1000 °C, 1 h, AC)+(850 °C, 2 h, AC) (AC means air-cooling). The alloy consists of three phases $(\alpha_2+\beta_2+O)$.

Square specimens with dimensions of 10 mm × 12 mm × 2 mm were cut by electrical-discharge method. Their surfaces were ground down to 800 grit SiC paper. Then, the specimens were degreased ultrasonically in acetone, cleaned by distilled water and dried in air prior to test. The specimens were heated to approximately 200 °C and then sprayed with a saturated aqueous solution of Na$_2$SO$_4$ to generate a continuous thin layer of sodium sulphate with a loading of about 3 mg/cm^2 (such loading was measured by an electrical analysis balance and determined by the mass change per unit area). The isothermal mass change measurements were conducted at 910 and 950 °C in air for 10.5 and 12 h by using a continuous thermo-gravimetric method, which permits mass change measurement under corrosion conditions. The sample was suspended in a thermo balance with a Pt wire and its mass change was recorded automatically.

After the hot corrosion test, the specimens were rinsed in boiling distilled water to remove the remains of sulphate. The phase composition of corrosion product layer was identified by a step-scanning Rigaku D/max−2400 X-ray diffractometer (XRD; Tokyo, Japan) with a scanning rate of 2 (°)/min, using Cu target K$_\alpha$ radiation under 40 kV and 300 mA with a scanning step of 0.02°. The morphology observation of surface corrosion product was performed by using SUPRA35 scanning electron microscope (SEM, LEO, Oberkochen, Germany), equipped with an energy-dispersive spectroscopy (EDS, INCA, Oxford Instrument, Oxford, UK) system. Prior to the cross-section view, the surface

of corroded specimens was chemically plated with nickel to avoid the occurrence of crack or spallation of corrosion product during the grinding and polishing process.

3 Results

3.1 Kinetics of hot corrosion

Figure 1(a) shows the hot corrosion kinetic curves of specimens deposited with Na$_2$SO$_4$ thin film at 910 °C for 12 h and 950 °C for 10.5 h in air, respectively. In order to compare the corrosion rate with that under other conditions, the oxidation kinetic curves (Na$_2$SO$_4$-free) in temperature range of 800−1000 °C in air are plotted in Fig. 1(b) as well. It should be noted that both the kinetic curves of hot corrosion and that of oxidation were obtained by only one tested sample by in-situ recording its mass change continuously, so no error bars were provided. Because the test temperature is above the melting point of Na$_2$SO$_4$ (884 °C), the salt melts and covers the sample surfaces, resulting in a typical hot corrosion attack.
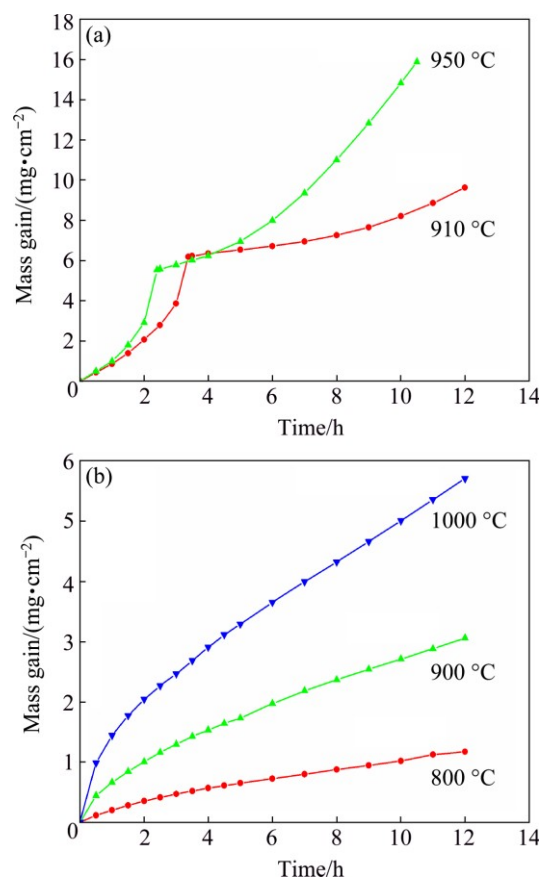

Fig. 1 Curves of mass gain per unit area vs time obtained at different temperatures: (a) Coated with thin film of Na$_2$SO$_4$; (b) Na$_2$SO$_4$-free (oxidation in air)

Very different from the oxidation kinetics, an obvious continuously accelerated characteristic appeared

for the cases of hot corrosion. The mass gain per unit area for the specimens in the presence of thin sodium sulphate film on their surfaces was much higher than that of the uncoated specimens. At approximately similar temperatures, the total mass gain after hot corrosion at 910 °C for 12 h was 9.632 mg/cm^2, much higher than that obtained after oxidation at 900 °C for 12 h (3.058 mg/cm^2). Meanwhile, the total mass gain after hot corrosion at 950 °C for 10.5 h was 15.881 mg/cm^2, nearly twice higher than that (5.704 mg/cm^2) obtained even at higher oxidation temperature and longer oxidation time (1000 °C for 12 h). So, the specimens suffered from severe hot corrosion attack in the presence of molten Na$_2$SO$_4$.

Figure 1(a) also suggests that in all runs the curves of mass changes versus time exhibit two regions of different kinetics. The first one corresponds to a very rapid mass gain kinetic and the second is a relatively slow one. For example, for the case of hot corrosion at 910 °C, the mass gain during the initial 3.5 h was 6.226 mg/cm^2, and its value was 3.404 mg/cm^2 for the following 8.5 h. For the case of hot corrosion at 950 °C, the mass gain for the initial 2.5 h was 5.582 mg/cm^2 and its value was 10.299 mg/cm^2 for the subsequent 8 h.

3.2 Phase identification of corrosion product

The XRD patterns of corrosion products formed on the surfaces of the tested specimens are presented in Fig. 2. XRD analysis revealed that, for all the specimens, the main crystalline phase was a mixture corrosion product of Nb$_2$O$_5$, TiO$_2$ and Al$_2$O$_3$. In both cases, the residual sodium sulphate was detected as well, indicating that no depletion of sodium sulphate occurred during the hot corrosion process.
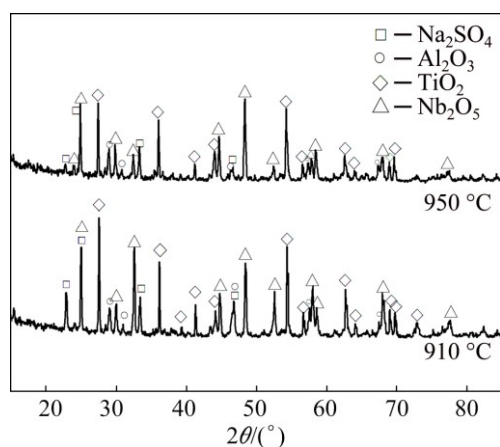

Fig. 2 XRD patterns of corrosion products for specimens coated with thin film of Na$_2$SO$_4$ after hot corrosion attack at 910 and 950 °C

3.3 Microstructure of corrosion product

Surface morphologies of the specimens coated with 3 mg/cm^2 Na$_2$SO$_4$ after hot corrosion at 910 and 950 °C in air are shown in Fig. 3. In both cases, thick corrosion product covered the surfaces of test specimens, and the straw-like corrosion products in microstructure appeared in the relatively flat regions (see Figs. 3(b) and (e), respectively). According to the results of both XRD and EDS analysis, such corrosion products were reasonably identified as TiO$_2$. It was apparent that numerous nodules appeared on the surfaces of specimens, as shown in Figs. 3(a) and (d). It seemed that the number of nodules increased with increasing temperature. The top of nodules exhibited much finer microstructure (see Figs. 3(c) and (f)).

3.4 Cross-section views of corrosion product

Figure 4 illustrates the cross-section views of specimens after hot corrosion at 910 °C for 12 h and 950 °C for 10.5 h, respectively. It was evident that a crevice gap existed along the interface between the internal corrosion product layer and the substrate, resulted from the mechanical preparation process of specimens. The thickness of corrosion product increased with increasing temperature. In both cases, a multi-layered corrosion product was produced. The outermost layer and the intermediate one were relatively loose and porous. Meanwhile, some continuous crevice bands and pores were observed. The inner layer corrosion scale near the alloy was relatively continuous and compact, mainly consisting of a mixture of TiO$_2$ and Nb$_2$O$_5$, which was attributed to the insufficiency or depletion of Al content in the substrate during the hot corrosion process. For the multi-layered microstructure, the gray-white phase mainly consisted of Nb$_2$O$_5$, the black one was Al$_2$O$_3$ and the gray one was TiO$_2$. According to Figs. 4(b) and (d), it was found that the bottom of the produced nodules was embedded into the substrate, causing the formation of pits beneath the interface of corrosion product/substrate.

4 Discussion

Because of the importance of hot corrosion in science and practical engineering, the aspects of its mechanism are investigated widely by various ways. It is well known that a fluxing mechanism is proposed for explaining the hot corrosion of alloys [29,31,32]. It is accepted that the major procedure of hot corrosion is that the oxides formed on the alloy surface can dissolve into the molten salt and a new oxide layer is produced by the process of re-precipitation. The way of dissolution depends on the melt basicity or the melt acidity induced by the reaction of a metal with sulphate and the removal of sulfur from the melt or the reaction of oxides with the molten salt.
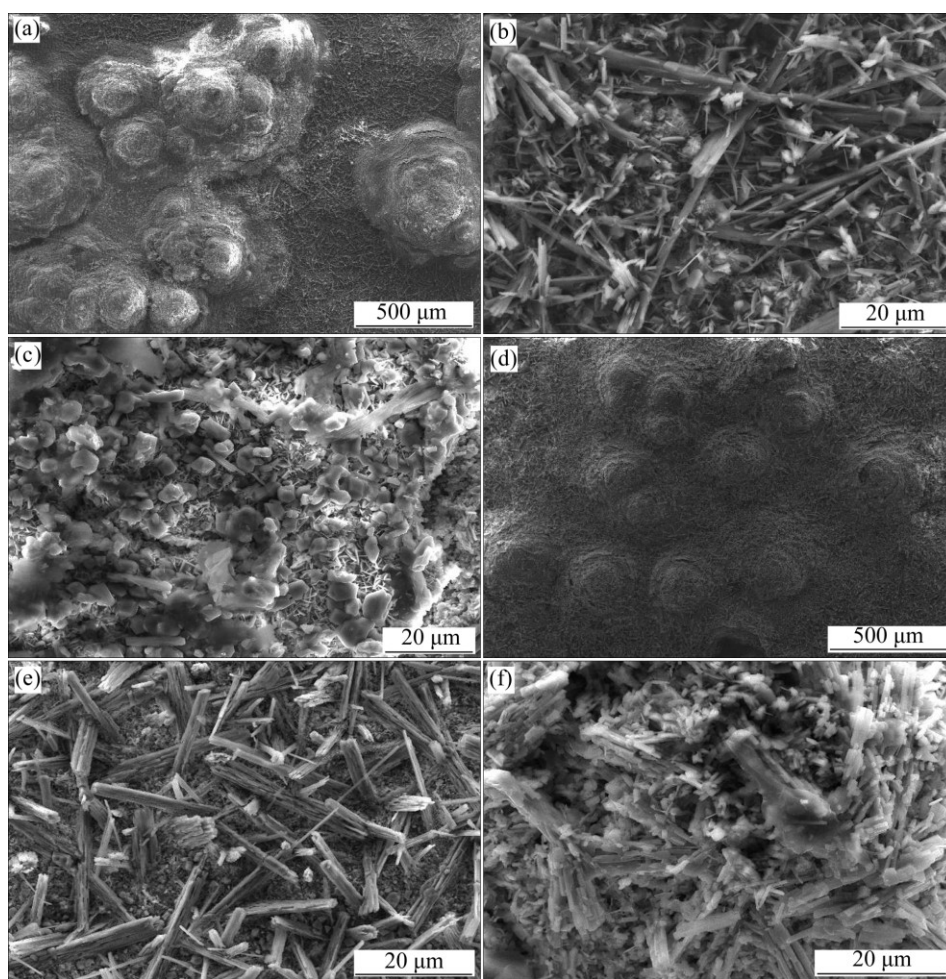
Fig. 3 SEM surface morphologies of tested specimens coated with thin film of 3 mg/cm² Na₂SO₄ after hot corrosion attack in air at 910 °C (a−c) and 950 °C (d−f)
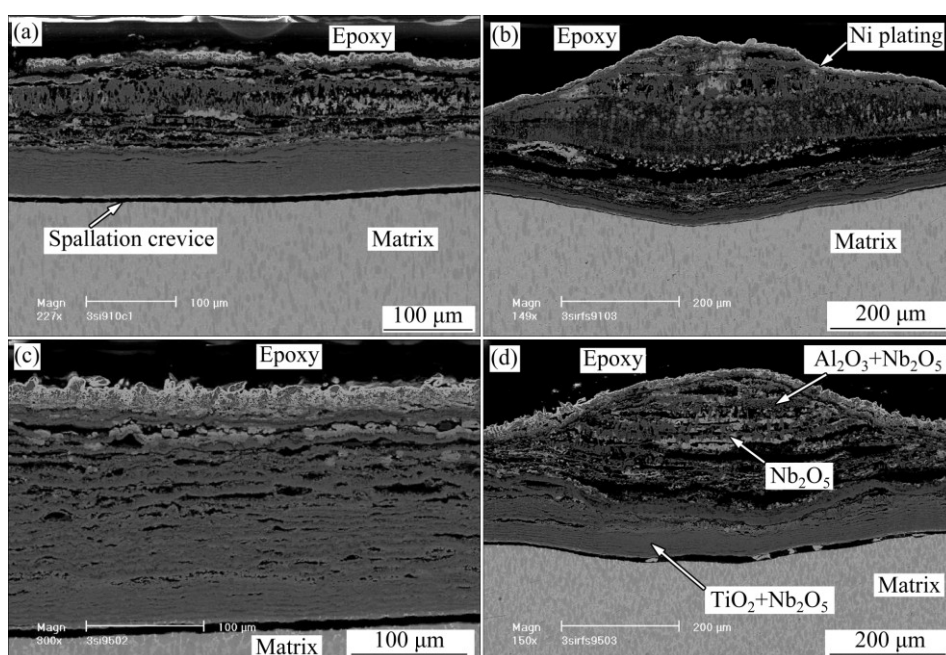

Fig. 4 Cross-section views of specimens coated with 3 mg/cm² Na₂SO₄ after hot corrosion in air: (a) Flat region at 910 °C; (b) Nodule at 910 °C; (c) Flat region at 910 °C; (d) Nodule at 950 °C

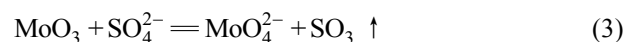In molten Na_2SO_4, the following chemical reactions occur, as expressed as

$$Na_2SO_4 = Na_2O + SO_3 \uparrow \tag{1}$$

$$SO_3 = 1/2S_2 + 3/2O_2 \uparrow \tag{2}$$

where Na_2O is basic component and SO_3 is acidic component.

Commonly, alloys bearing some refractory alloying elements, such as Mo, W or V, will suffer from accelerated acidity dissolution corrosion because their corresponding refractory oxides will react with molten Na_2SO_4, resulting in sufficient melt acidity to promote the acidity dissolution corrosion.

For the tested alloy, the oxides of Mo or V formed at high temperatures will react with molten Na_2SO_4 as the following reactions:

$$MoO_3 + SO_4^{2-} = MoO_4^{2-} + SO_3 \uparrow \tag{3}$$

$$V_2O_5 + SO_4^{2-} = 2VO_3^- + SO_3 \tag{4}$$

Considering the equilibrium relationship between O^{2-} and SO_3 / SO_4^{2-}, Eqs. (3) and (4) can be expressed further as, respectively:

$$MoO_3 + O^{2-} = MoO_4^{2-} \tag{5}$$

$$V_2O_5 + O^{2-} = 2VO_3^- \tag{6}$$

Equations (5) and (6) will consume O^{2-} at molten sulphate/alloy interface and result in the acidity dissolution of oxides in molten Na_2SO_4. Under such a condition, the main mixture oxides formed on the surface of tested specimens, such as Al_2O_3, TiO_2 and Nb_2O_5, will dissociate according to Eqs. (7) to (9) [33]:

$$Al_2O_3 = 2Al^{3+} + 3O^{2-} \tag{7}$$

$$TiO_2 = Ti^{4+} + 2O^{2-} \tag{8}$$

$$Nb_2O_5 = 2Nb^{5+} + 5O^{2-} \tag{9}$$

Meanwhile, due to the existing concentration gradient, the produced Al^{3+}, Ti^{4+}, Nb^{5+}, MoO_4^{2-} and VO_3^- will diffuse outwardly from the oxide/molten interface toward the molten/air interface. On the outside surface, MoO_4^{2-} and VO_3^- will evaporate as the form of corresponding oxides due to their high vapor pressure and such process will release O^{2-} further. The increasing O^{2-} will lead to the high O^{2-} activity on the outer surface. Because of the negative gradient of acidity from the inside to the outside interface, i.e., oxide/molten interface to molten/air interface, the outward diffusing solute in the molten sulfate will re-precipitate to form corresponding oxides subsequently, i.e., the oxides of TiO_2, Al_2O_3 and Nb_2O_5 will re-precipitate at the molten sulphate/air interface in the end. The re-precipitation process of soluble oxide in the sulphate results in a loose and porous corrosion product. The possible reactions are described as follows:

$$2Al^{3+} + 3O^{2-} = Al_2O_3 \tag{10}$$

$$Ti^{4+} + 2O^{2-} = TiO_2 \tag{11}$$

$$2Nb^{5+} + 5O^{2-} = Nb_2O_5 \tag{12}$$

During such a process, the dissolution of refractory oxides such as MoO_3 and V_2O_5 at interface of alloy/molten sulphate and their evaporation at the molten sulphate/air interface sustain the necessary activity of O^{2-} in the molten sulphate. So, the accelerated corrosion for the acidity fluxing will be "self-sustained", because the refractory MoO_3 and V_2O_5 can be produced continuously near the interface of alloy/molten sulphate.

The refractory oxides of MoO_3 and/or V_2O_5 can be formed during the transient oxidation stage together with other stable oxides, or be produced on some local sites enriched with Mo or V on the substrate, or the combination of them. The observation of surface morphologies and cross-sections of corrosion product showed that some corrosion product nodules appeared on the surface after hot corrosion attack. The reason is that some local locations enriched with Mo and/or V will predominantly produce more MoO_3 and/or V_2O_5 during the initial oxidation procedure. Once the necessary melt acidity condition for the accelerated acidity fluxing is triggered, the corrosion for these local locations will be accelerated and the nodules with accumulated corrosion products will be formed. In detail, the formation process of corrosion product nodules can be divided into four stages and can be described according to the illustrative schematics in Fig. 5.

Stage I: Segregation of refractory alloying elements such as Mo and/or V occurs, resulting from local enrichment of these elements at some sites caused possibly by the content fluctuation of alloying elements.

Stage II: The refractory alloying elements such as Mo and/or V are oxidized and transformed into their corresponding refractory oxide, e.g., MoO_3 and/or V_2O_5, under the molten sodium sulphate film. More refractory oxides are generated due to the enrichment of refractory alloying elements on those segregation sites. Meanwhile, a mixture oxide mainly consisting of TiO_2, Al_2O_3 and Nb_2O_5 is produced.

Stage III: The reactions between the refractory oxides and molten sulphate according to Eqs. (3) and (4) and the subsequent solute diffusion toward the interface of molten sulphate/air result in increasing melt acidity near the interface of molten sulphate and substrate. Especially, severer melt acidity is produced on those sites with segregation of refractory elements due to the sufficient supply of refractory oxides.

Stage IV: The mixture oxides of Al_2O_3, TiO_2, Nb_2O_5 will dissolve into the molten sulphate according to Eqs. (7) to (9) and re-precipitate in the form of loose and
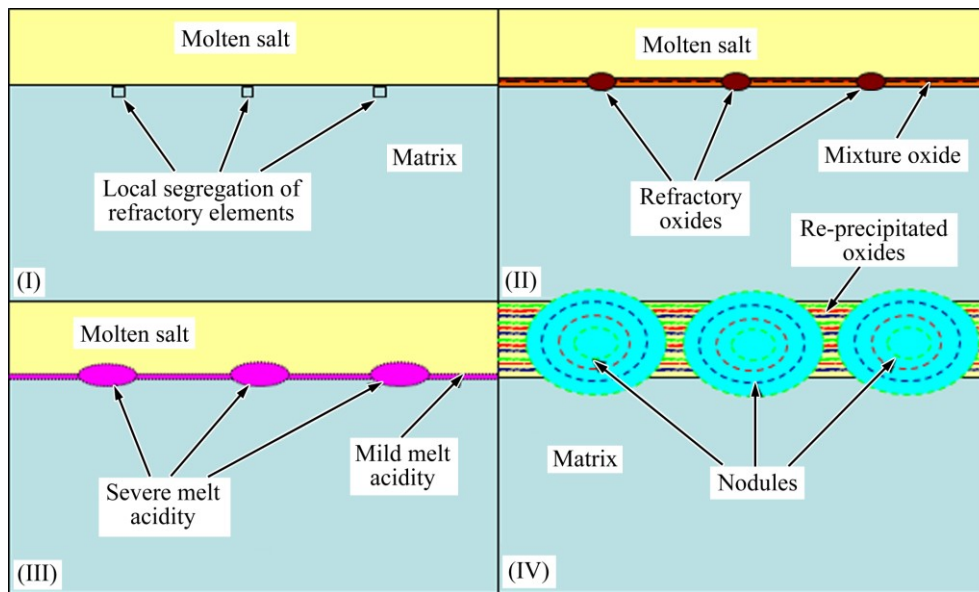
Fig. 5 Illustrative schematic of formation process of corrosion production nodules for specimens deposited with thin Na_2SO_4 film after hot corrosion in air

porous oxides on the outer side of the molten sulphate according to Eqs. (10)−(12). Because of the severe melt acidity established around the segregation sites of refractory elements, more mixture oxides will be dissolved into molten sulphate, and correspondingly, more re-precipitated mixture oxides will be formed. Continuous accumulation of such a process gives rise to the formation of corrosion product nodules.

The kinetic curves of hot corrosion in Fig.1 exhibit the initial rapid stage followed by the subsequent relatively slow one. This could be attributed to the behaviour of refractory alloying elements in the substrate as well. As illustrated in Fig. 5, during stage III, the severe melt acidity on some segregation sites of refractory elements leads to a stronger acidity fluxing of mixture oxides. The accelerated dissolution of mixture oxides and their re-precipitation due to the severe melt acidity cause a sharp increase of mass gain, corresponding to the initial rapid stage. After that period, a relatively mild melt acidity gives rise to a relatively slow kinetics.

In fact, the activity of acidic component resulted from the dissolution of refractory oxides at oxide/molten sulphate interface is higher than that at the molten sulphate/air interface, so the solubility of protective oxide at oxide/molten sulphate interface is higher than that at the sulphate/air interface. A negative gradient of solubility of oxide exists in the molten sulphate [34]:

$$\left(\frac{d[MO]}{dx} \right)_{x=0} < 0 \tag{13}$$

where [MO] is the solubility of protective oxide in

molten sulphate, and x is the distance between oxide/ molten sulphate interface and the molten sulphate/air interface. It is accepted that Eq. (13) is the necessary condition for the continuous hot corrosion procedure.

Usually, an incubation period with extremely low corrosion rate may occur during the hot corrosion procedure in the presence of molten Na_2SO_4 salt. From the hot corrosion kinetic curves illustrated in Fig. 1, almost no such incubation period is observed. The reason is that after the transient oxidation stage, the refractory oxides such as MoO_3 and V_2O_5 are formed. They react with the molten Na_2SO_4, resulting in an increasing acidity in the melt. Once a critical condition for the acidity fluxing of hot corrosion is triggered, a corresponding accelerated corrosion stage will appear.

5 Conclusions

1) Compared with the mass gain per unit area during oxidation (Na_2SO_4-free) at various temperatures in air, the Ti−24Al−14Nb−3V−0.5Mo−0.3Si (mole fraction, %) alloy coated with 3 mg/cm^2 Na_2SO_4 salt film suffered from significant hot corrosion attack at 910 and 950 °C in air. The mass changes versus time curves exhibited two regions of different kinetics and almost no incubation period was observed.

2) A mixture of oxides with main crystalline phases of TiO_2, Nb_2O_5 and Al_2O_3 corrosion product was formed during the hot corrosion. Disperse corrosion product nodules appeared on the surfaces of specimens after the hot corrosion attack.

3) The hot corrosion procedure was described

according to the fluxing mechanism of acidity molten. During the corrosion process, the refractory oxides played a significantly important role in determining the development of hot corrosion attack.

References

[1] FENG Guang-jie, LI Zhuo-ran, FENG Shi-cheng, SHEN Zhong-ke. Effect of Ti−Al content on microstructure and mechanical properties of C$_f$/Al and TiAl joint by laser ignited self-propagating high-temperature synthesis [J]. Transactions of Nonferrous Metals Society of China, 2015, 25: 1468−1477.

[2] LI Yong-quan, XIE Fa-qin, WU Xiang-qing. Microstructure and high temperature oxidation resistance of Si−Y co-deposition coatings prepared on TiAl alloy by pack cementation process [J]. Transactions of Nonferrous Metals Society of China, 2015, 25: 803−810.

[3] FANG Lu, DING Xian-fei, HE Jian-ping, ZHANG Lai-qi, LIN Zhi, LIN Jun-pin. Microstructure instability of fully lamellar TiAl alloy containing high content of Nb after long-term thermal cycling [J]. Transactions of Nonferrous Metals Society of China, 2014, 24: 3095−3102.

[4] SUBRAHMANYAM J. Cyclic oxidation of aluminized Ti−14Al−24Nb alloys [J]. Journal of Material Science, 1988, 23: 1906−1910.

[5] POLMEAR I J. Recent development in light alloys [J]. Mater Trans JIM, 1996, 37: 12−31.

[6] DJANARTHANY S, VIALA J C, BOUIX J. An overview of monolithic titanium aluminides based on Ti$_3$Al and TiAl [J]. Mater Chem Phys, 2001, 72: 301−319.

[7] GABBITAS B, CAO P, RAYNOVA S, ZHANG D. Microstructural evolution during mechanical milling of Ti/Al powder mixture and production of intermetallic TiAl cathode target [J]. J Mater Sci, 2012, 47: 1234−1243.

[8] SRINIVASARAO B, ZHILYAEV A P, MUNOZ-MORENO R, PEREZ-PRADO M T. Effect of high pressure torsion on the microstructure evolution of a gamma Ti−45Al−2Nb−2Mn−0.8vol% TiB$_2$ alloy [J]. J Mater Sci, 2013, 48: 4599−4605.

[9] SIMOES S, VIANA F, VENTZKE V, KOCAK M, RAMOS A S, VIEIRA M T, VIEIRA M F. Diffusion bonding of TiAl using Ni/Al multilayers [J]. J Mater Sci, 2010, 45: 4351−4357.

[10] KOO C H, YU T H. Pack cementation coatings on Ti$_3$Al−Nb alloys to modify the high-temperature oxidation properties [J]. Surf Coat Technol, 2000, 126: 171−180.

[11] LUTHRA K L. Stability of protective oxide films on Ti-base alloys [J]. Oxid Met, 1991, 36: 475−490.

[12] PERKINS R A, CHIANG K T, MEIER G H. Formation of alumina on Ti−Al alloys [J]. Scripta Metall, 1987, 21: 1505−1510.

[13] MEIER G H, APPALONIA D, PERKINS R A, CHIANG K T. Oxidation of titanium-base alloys [C]//GROBSTEIN T, DOYCHAK J. Oxidation of High Temperature Intermetallics. Ohio: TMS, 1989: 185−193.

[14] RAHMEL A, SPENCER P J. Thermodynamic aspects of TiAl and TiSi$_2$ oxidation: The Al−Ti−O and Si−Ti−O phase-diagrams [J]. Oxid Met, 1991, 35: 53−68.

[15] KUMARI S V, LITTLE J A. Hot-salt oxidation characteristics of titanium aluminides [J]. Journal of Materials Science, 1998, 33: 4315−4319.

[16] CHANG S Y. The isothermal and cyclic oxidation behavior of a titanium aluminide alloy at elevated temperature [J]. Journal of Materials Engineering and Performance, 2007, 16: 508−514.

[17] ZHU Ming, LI Mei-shuan, LI Ya-li, ZHOU Yan-chun. Influence of sol–gel derived Al$_2$O$_3$ film on the oxidation behavior of a Ti$_3$Al based alloy [J]. Mater Sci and Eng A, 2006, 415: 177−183.

[18] ZHANG Z G, WANG Y J, XIAO L J, ZHANG L Q, SU Y, LIN J S. High-temperature oxidation of hot-dip aluminizing coatings on a Ti$_3$Al−Nb alloy and the effects of element additions [J]. Corrosion Science, 2012, 64: 137−144.

[19] BROTZU A, FELLI F, PILONE D. Effect of alloying elements on the behaviour of TiAl-based alloys [J]. Intermetallics, 2014, 54: 176−180.

[20] AKAI M, FANIGUCHI S, SHIBATA T. Oxidation characteristics of Ti−14Al−21Nb alloy at different temperatures in purified oxygen [J]. J Jpn Inst Met, 1994, 58: 1169−1176.

[21] WELSCH G, KAHVECI A I. Oxidation behavior of titanium aluminide alloys [C]//GROBSTEIN T, DOYCHAK J. Oxidation of High Temperature Intermetallics. Ohio: TMS, 1989: 207−218.

[22] PERKINS R A, CHIANG K T. Formation of alumina on niobium and titanium alloys [C]//GROBSTEIN T, DOYCHAK J. Oxidation of High Temperature Intermetallics. Ohio: TMS, 1989: 157−169.

[23] FANG W, KO S H, HASHIMOTO H, ABE T, PARK Y H. High temperature oxidation behavior of Ti$_3$Al−Nb alloys prepared by pulse discharge sintering [J]. Mater Sci Eng A, 2002, 329: 708−712.

[24] QIAN Yu-hai, LI Mei-shuan, LU Bin. Isothermal oxidation behavior of Ti$_3$Al-based alloy at 700−1000 °C in air [J]. Transactions of Nonferrous Metals Society of China, 2009, 19: 525−529.

[25] QIU G H, WU J S, ZHANG L T, LIN T L. Oxidation behavior of Ti$_3$Al alloyed with niobium and silicon [J]. Scripta Metallurgica et Materialia, 1995, 33: 213−217.

[26] WU J S, ZHANG L T, WANG F, JIANG K, QIU G H. The individual effects of niobium and silicon on the oxidation behaviour of Ti$_3$Al based alloys [J]. Intermetallics, 2000, 8: 19−28.

[27] YANG K L, HUANG J C, CHEN S C. Mechanical anisotropy of superplastic Ti$_3$Al based alloy [J]. Key Eng Mater, 2004, 274−276: 295−300.

[28] KHOBAIB M, VAHLDIE F W. High temperature oxidation behavior of Ti$_3$Al alloys [C]//FROES F H, CULL R A. Space Age Metals Technology. Covina: Society for the Advancement of Material and Process Engineering, 1988: 262−270.

[29] RAPP R A. Hot corrosion of materials: A fluxing mechanism? [J]. Coros Sci, 2002, 44: 209−221.

[30] GURRAPPA I. Mechanism of degradation of titanium alloy IMI 834 and its protection under hot corrosion conditions [J]. Oxid Met, 2003, 59: 321−332.

[31] GOEBEL J A, PETTIT F S. Na$_2$SO$_4$-induced accelerated oxidation (hot corrosion) of nickel [J]. Met Trans, 1970, 1: 1943−1954.

[32] GOEBEL J A, PETTIT F S, GOWARD G W. Mechanisms for the hot corrosion of nickel-base alloys [J]. Metall Trans, 1973, 4: 261−278.

[33] TURKDOGAN E T. Physical chemistry of high temperature technology [M]. London: Academic Press, 1980.

[34] RAPP R A, GOTO K S. The hot corrosion of metals by molten salts [C]//Proceedings of the Second International Symposium on Molten Salts. Pennington, NJ: Physical Electrochemistry Devision Electrochemical Society, 1981.

表面涂 Na_2SO_4 盐膜的改性 Ti_3Al 基合金在 910 和 950 °C 空气中的热腐蚀行为

钱余海 [1]，李希超 [1,2]，李美栓 [1]，徐敬军 [1]，卢　斌 [1]

1. 中国科学院 金属研究所 沈阳材料科学(国家)联合实验室，沈阳　110016；
2. 中国科学院大学，北京　100039

摘　要：研究表面涂 Na_2SO_4 盐膜的改性 Ti_3Al 基合金在 910 和 950 °C 空气中的热腐蚀行为，并分别采用 XRD 和 SEM 等测试技术分析腐蚀产物的物相组成，观察腐蚀产物表面及截面的形貌特征。原位热重分析结果表明合金遭受了严重的热腐蚀，腐蚀动力学曲线表现出两个阶段的特征，腐蚀产物膜由疏松多孔的 TiO_2、Nb_2O_5 和 Al_2O_3 混合氧化物组成。热腐蚀过程中合金表面形成了大量的瘤状产物，绘制了详细描述这些瘤状产物形成及发展过程的示意图。由于局部的酸性溶解过程，难熔金属氧化物对热腐蚀过程的发展具有决定性作用。

关键词：改性 Ti_3Al 基金属间化合物；热腐蚀；腐蚀产物瘤；Na_2SO_4 盐膜

(Edited by Wei-ping CHEN)